Identification and Acute Targeting of Gaps in Atrial Ablation Lesion Sets Using a Real-Time Magnetic Resonance Imaging System

Ravi Ranjan, MD, PhD; Eugene G. Kholmovski, PhD; Joshua Blauer, BS;
Sathya Vijayakumar, MS; Nelly A. Volland, PhD; Mohamed E. Salama, MD;
Dennis L. Parker, PhD; Rob MacLeod, PhD; Nassir F. Marrouche, MD

Background—Radiofrequency ablation is routinely used to treat cardiac arrhythmias, but gaps remain in ablation lesion sets because there is no direct visualization of ablation-related changes. In this study, we acutely identify and target gaps using a real-time magnetic resonance imaging (RT-MRI) system, leading to a complete and transmural ablation in the atrium.

Methods and Results—A swine model was used for these studies (n=12). Ablation lesions with a gap were created in the atrium using fluoroscopy and an electroanatomic system in the first group (n=5). The animal was then moved to a 3-tesla MRI system where high-resolution late gadolinium enhancement MRI was used to identify the gap. Using an RT-MRI catheter navigation and visualization system, the gap area was ablated in the MR scanner. In a second group (n=7), ablation lesions with varying gaps in between were created under RT-MRI guidance, and gap lengths determined using late gadolinium enhancement MR images were correlated with gap length measured from gross pathology. Gaps up to 1.0 mm were identified using gross pathology, and gaps up to 1.4 mm were identified using late gadolinium enhancement MRI. Using an RT-MRI system with active catheter navigation gaps can be targeted acutely, leading to lesion sets with no gaps. The correlation coefficient (R^2) between the gap length was identified using MRI, and the gross pathology was 0.95.

Conclusions—RT-MRI system can be used to identify and acutely target gaps in atrial ablation lesion sets. Acute targeting of gaps in ablation lesion sets can potentially lead to significant improvement in clinical outcomes. (***Circ Arrhythm Electrophysiol***. 2012;5:1130-1135.)

Key Words: ablation ■ magnetic resonance imaging ■ atrial fibrillation arrhythmia ■ real time magnetic resonance imaging ■ real-time imaging

Radiofrequency ablation is routinely used to target numerous cardiac arrhythmias, such as ventricular tachycardia and atrial fibrillation.[1,2] In many of these procedures, the goal of the ablation procedure is to electrically isolate one region of the myocardium from another.[3] When ablating for atrial fibrillation, the goal is to achieve electric isolation of the pulmonary veins.[4] Yet, despite the best efforts, the success rate for some ablation procedures like those for atrial fibrillation ranges from 40% to 80%.[5,6] One of the reasons for the low procedural success is the presence of gaps in ablation lesion sets.[7–9] In the current ablation procedures, there is no direct visualization of changes in the tissue, and ablation is inferred based on numerous indirect parameters, such as local electrogram attenuation, power delivered, and temperature at the catheter tip. None of these are completely reliable measures of ablation and can result in ablation lesions sets with gaps.

Magnetic resonance imaging (MRI) has excellent soft tissue visualization capability, which can be used to identify ablation lesions.[10,11] Here, we report using MRI to acutely identify ablation lesions and accurately determine gaps in ablation lesion sets. We then describe using a real time MRI system to acutely target and ablate these gap areas in the ablation lesion set. In addition, we characterize the smallest gaps that can be identified using the real-time MRI system. A method to identify ablation lesions and gaps in between them and the ability to target these gaps acutely can potentially result in significant improvement in the outcome of these procedures.

Clinical Perspective on p 1135

Methods

Animal Preparation

A swine model was used for the study. The Institutional Animal Care and Use Committee approved the study. Animals weighing 30 to 35 kg (n=12) were used and were given a preanesthetic cocktail of telazol 4.4 mg/kg, ketamine 2.2 mg/kg, and xylazine 2.2 mg/kg intramuscularly. For anesthesia, 20 to 40 minutes later they were given

20 to 60 mg/kg of pentobarbital intravenously. They were maintained in deep anesthesia by giving periodic intravenous injections of 30 to 40 mg/kg of pentobarbital. The animals were mechanically ventilated. Venous access to the femoral veins and femoral artery was obtained by a cut-down approach to the blood vessels. Sheaths of 11F (St Jude Medical, Austin, TX) were placed in the right and left femoral vein and were used to insert the mapping and ablation catheter. A 6F sheath was placed in the right femoral artery and was used for blood pressure monitoring and for obtaining periodic arterial sample for arterial blood gas analysis during the study. Two groups of animals were used for the study. After being anesthetized, the animals in the first group (n=5) were taken to the electrophysiology laboratory with a fluoroscopy system, and ablation lesions were created as described below. The animals in the second group (n=7) were taken directly to the real-time MRI (RT-MRI) system after being anesthetized for ablation and identification of the gap as described in the section Visualizing Gap Between Ablation Lesions Using MRI.

Electrophysiology Studies Using Fluoroscopy

Anesthetized animal from the first group (n=5) was moved to the electrophysiology laboratory with a fluoroscopy (Artis Zeego; Siemens USA, Malvern, PA) and an electroanatomic mapping system. CARTO (Biosense Webster, Diamond Bar, CA) electroanatomic mapping system was used for electrophysiology studies. A nonirrigated 4-mm-tip NaviStar (Biosense Webster) catheter was used for electroanatomic mapping. The catheter was advanced to the right atrium (RA) via the sheath in the right femoral vein. A baseline voltage map of the RA was made. Two discrete ablation lesions were made in the RA spaced about a centimeter apart. Ablation was done in a temperature-controlled mode with a 60° cut-off and a power of 30 W for 30 seconds. After the ablation, a new voltage map was created to confirm the low-voltage areas in the ablated areas and normal voltage in the gap in between. After the electrophysiology study, the NaviStar catheter was removed and the animal was checked to make sure it was free of any ferromagnetic materials. It was then moved to the MR scanner.

Electrophysiology Study in the MRI Scanner

After the ablation in the fluoroscopy suite, the animal was moved to the MRI suite with a 3-tesla MRI scanner (Verio; Siemens Healthcare, Erlangen, Germany). MRI-compatible ECG electrodes were put on the chest and connected to an MRI-compatible monitoring system (Veris MR; Medrad Inc, Warrendale, PA) for ECG, blood pressure, and oxygen saturation monitoring. The total time from the end of ablation in the fluoroscopy suite to the beginning of MR image acquisition was less than an hour. A gadolinium-based MRI contrast agent (Multihance; Bracco Diagnostic Inc, Princeton, NJ) was injected, and magnetic resonance angiogram (MRA) of the whole heart was acquired. MRA was performed during slow infusion of gadolinium-based contrast agent (dose=0.15 mmol/kg; infusion rate=0.1 mmol/s; Multihance; Bracco Diagnostic Inc). MRA images were acquired using a 3-dimensional (3D) respiratory navigated and ECG-gated gradient-recalled echo pulse sequence, with echo time/repetition time of 1.3/2.9 ms, flip angle of 23°, bandwidth of 870 Hz/pixel, field of view (FOV) of 240×240×120 mm, matrix size of 192×192×48, 25% oversampling in slice-encoding direction, voxel size of 1.25×1.25×2.5 mm, and phase-encoding direction of left to right. The data acquisition was limited to 20% of cardiac cycle and was performed during the stationary (diastolic) phase of RA. Twenty minutes after contrast injection, late gadolinium enhancement (LGE) images with spatial resolution of 1.25×1.25×2.5 mm were acquired. The LGE images were acquired using a 3D respiratory-navigated, inversion recovery–prepared gradient-recalled echo pulse sequence with echo time of 1.4 ms, repetition time of 3.1 ms, flip angle of 14°, bandwidth of 780 Hz/pixel, FOV of 240×240×110 mm, matrix size of 192×192×40, 10% oversampling in slice-encoding direction, voxel size of 1.25×1.25×2.5 mm, and phase-encoding direction of left to right. Inversion pulse was applied to every heart beat, and fat

saturation was applied immediately before data acquisition. Timing for data acquisition was found from cine images of RA. The data acquisition was limited to 15% of cardiac cycle and was performed during the stationary phase of RA.

The RA geometry was segmented from the MRA image volume using Seg3D 2.0 (Scientific and Computing Institute, University of Utah). Specifically, the contrast-enhanced blood pool was isolated using a user-defined threshold. A surface mesh of the RA was then generated from the segmentation using SCIRun 4.6 (Scientific and Computing Institute, University of Utah). The ablation lesions were observed and segmented from the LGE-MRI scan using Seg3D 2.0 based on acute contrast enhancement. Geometric models of the lesions were then created using SCIRun 4.6 and imported concurrently with the MRA-derived RA model in the real-time MRI visualization and navigation interface interactive front end (Siemens Corporate Research, Princeton, NJ). RT-MRI guidance of the catheter movement during mapping and ablation was provided by the interactive real-time tip tracking pulse sequence and the interactive front end navigation and visualization software (Siemens Corporate Research, Princeton, NJ). The catheter was visualized during navigation with an RT-MRI sequence (radiofrequency-spoiled gradient-recalled echo pulse sequence with a frame rate of ≈5 frames per second), and 4 tracking microcoils near the tip of the custom MRI-compatible catheter (MRI Interventions Inc, Irvine, CA) allowed for accurate detection of the catheter position in 3D space. Real-time images were acquired sequentially in multiple slices and rendered in 3D at their respective locations. Typical scan parameters for RT sequence were as follows: echo time, 1.5 ms; repetition time, 3.3 ms; flip angle, 13°; bandwidth, 750 Hz/pixel; spatial resolution, 1.8×2.0 mm; and slice thickness, 5 mm.

An 8F, 3-tesla MR-compatible, irrigated, temperature sensing, mapping, and ablation catheter (MRI Interventions, Irvine, CA), described earlier,[12] was inserted into the RA via the right femoral vein. The RT-MRI visualization interface with the shell of the RA was used to guide the catheter movement, along with the surface ECG and intracardiac electrograms recorded by the catheter. The tip of the catheter was positioned on the more cranial lesion, and under RT-MRI guidance the gap area between the 2 lesions was ablated. The MRI-compatible catheter was connected to a standard radiofrequency ablation unit (Stockert-70, radiofrequency generator; Biosense Webster) with custom-built interface for the MRI-compatible catheters. A power setting of 30 W was used to ablate in the atrium. After ablation in the MR scanner, gadolinium contrast agent was infused again and LGE images were acquired. After imaging, the animals were injected with triphenyltetrazolium chloride and the animals were euthanized with intravenous potassium chloride. Triphenyltetrazolium chloride stains live tissue red in color, clearly demarcating ablated and infarcted areas.[13,14] The animal chest was opened and the heart excised for further examination. The endocardial surface of the RA was exposed by making a linear incision from the inferior to the superior vena cava. The ablated lesions were visually inspected, and tissues were excised for histology.

Visualizing Gap Between Ablation Lesions Using MRI

For this part of the project, the second set of animals (n=7) were prepared as described above, except that instead of making lesions in the fluoroscopy suite, the animals were taken directly to the MRI scanner. MRA was acquired using a gadolinium-based contrast agent, as described above. From the MRA images, the RA was segmented and meshed (using Seg3D 2.0 and SCIRun 4.6, respectively) and imported in the real-time catheter visualization software interface. MRI-compatible catheter described above was inserted in the right femoral vein and advanced to the RA using RT-MRI guidance. Using the segmented shell of the RA and with RT-MRI guidance, discrete ablation lesions were made in the RA. To minimize the number of animals, paired lesions with varying gaps between the ablation lesions were made in distinct parts of the RA. These lesions were made in the temperature-controlled mode set at 60° and 30 W. The ablation was carried out for 30 seconds. After the lesions were made,

3D LGE MR images were acquired. The LGE images had a spatial resolution of $1.0 \times 1.0 \times 1.5$ mm. Subsequently, triphenyltetrazolium chloride was injected, and the animal was euthanized using intravenous potassium chloride. The chest was opened and the heart excised for further examination. The gap between the lesions was measured on the endocardial surface. Eight of the ablated lesion pairs with the gap in between underwent hematoxylin and eosin and Masson trichrome staining to further characterize the gap and the ablated areas. For histology, the tissue was fixed in formalin and then embedded in a paraffin block. Once embedded in the block, sections were obtained and stained with hematoxylin and eosin and Masson trichrome. The 3D LGE MR images were processed using Osirix (Osirix Imaging Software, Pixmeo, Geneva, Switzerland). A higher-resolution 3D data set with a resolution of $0.5 \times 0.5 \times 1.0$ mm was created by interpolating the data. The 3D image set was visualized using the 3D multiplanar reconstruction technique. The measurement tool was used to quantify the gap length between the ablation lesions.

Statistical Analysis

The gap length between the ablation lesions determined from the endocardial surface of gross pathology was correlated with the gap length determined from the 3D LGE MR images. The correlation coefficient was determined for the 2 measurements.

Results

Filing the Gap Using Real-Time MRI

At baseline, none of the animals showed any areas of low voltage in the RA. After obtaining a baseline voltage map, 2 discrete ablation lesions were made in the RA. The new voltage map created after the lesions showed discrete areas of low voltage at the ablation sites and normal voltage in the gap area between the lesions (online-only Data Supplement Figure I).

After creating the ablation lesions in the fluoroscopy suite, the animal was moved to the MR scanner. In the MR scanner, MRA and LGE images were acquired identifying the ablation lesions. Figure 1 depicts LGE images showing the 2 discrete lesions in the RA in the axial (A and B), coronal (C), and
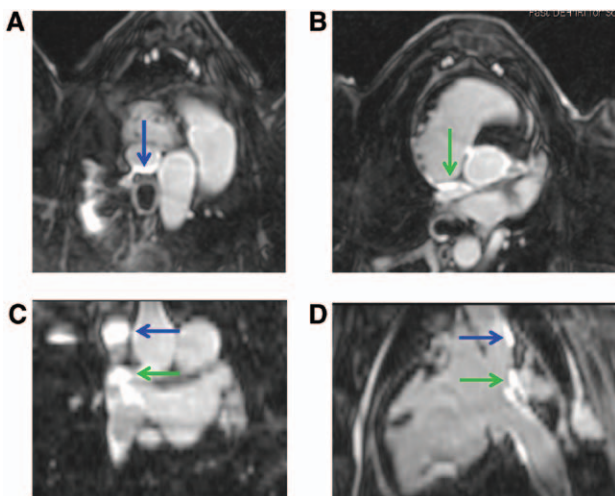
sagittal (D) planes. The MRA and LGE images were segmented to create a shell of the RA and identify ablated lesions with the gap in between. This image was uploaded in the real-time MRI visualization and navigation interface at the MR scanner. Figure 2 is a screen shot of the real-time navigation system in the MRI, showing the RA shell, the ablated lesions, and the catheter in between. The real-time navigation system was used to position the catheter at the previously ablated areas and guide its navigation to ablate the gap between the 2 lesions. In addition to using the RA shell, the location of the previously ablated lesions on the shell and real-time MR images through different planes and the lack of local bipolar electrogram were used to confirm the location of previously ablated areas. After ablating the gap area, the LGE images were reacquired, confirming that the gap between the previously ablated lesions was also ablated. Figure 3 illustrates LGE images with the gap area between the lesions ablated in axial (A and B), coronal (C), and sagittal (D) planes.

Gross Pathology and Histology

The RA tissue around the ablated area was excised for gross examination and histological examination. On gross examination, a continuous set of lesions was confirmed. Cut sections on gross pathology and Masson trichrome staining confirmed the ablation and its transmurality (online-only Data Supplement Figure II).

Minimum Gap Length Detected by MRI

Ablation lesions with varying distance between them were made in the RA. The gap length as measured in the endocardial surface was compared with the gap length as measured
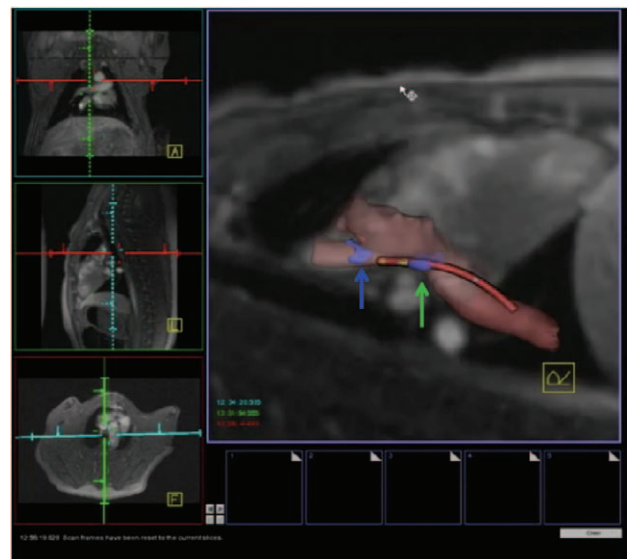

Figure 1. A and **B**, Axial late gadolinium enhancement cardiac magnetic resonance images showing the 2 ablation lesions in the posterior wall of the right atrium. **A** is more cranial of the 2 axial planes. **C**, A coronal section showing both the lesions. **D**, A sagittal section showing the 2 lesions. The cranial lesion is marked by a **blue arrow** and the caudal lesion is marked by a **green arrow**.

Figure 2. Screen shot of the real-time magnetic resonance imaging navigation system. On the **left** are 3 magnetic resonance images in 3 perpendicular planes. The location of these planes can be adjusted by the user for optimal performance. **Right**, A sagittal viewing plane with the shell of the right atrium (in orange) and the ablated lesions (marked in **purple with blue and green arrows**) imported to the real-time catheter navigation interface. In this image, the catheter tip is in the gap area between the 2 ablation lesions.
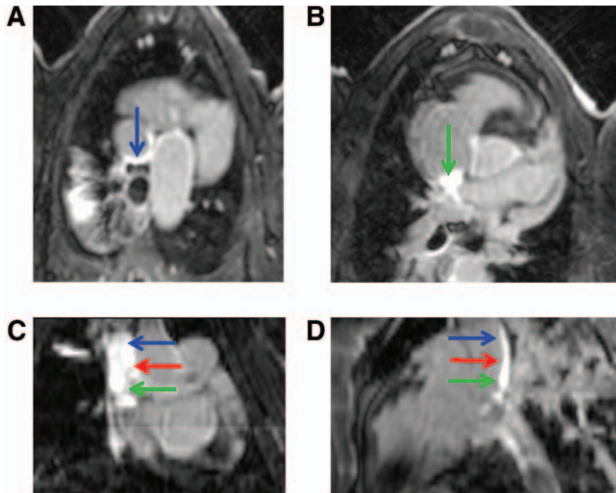
Figure 3. Late gadolinium enhancement magnetic resonance (MR) images acquired after ablating the gap between prior ablation lesions. **A** and **B**, Axial planes through the cranial (**A**) and caudal (**B**) ablation lesions. **C**, A coronal section showing that the gap area between the 2 lesions is also ablated (marked by **red arrow**). **D**, A sagittal section showing the continuous ablation line. The lesions made in the electrophysiology laboratory using fluoroscopy are marked by **blue** and **green arrows**, and the gap area ablated in the MR scanner using the real-time MR system is marked with **red arrow**.

in the 3D LGE MR image set. Figure 4 shows a typical MR image of a pair of ablation lesion with the gap in between. Figure 4A and 4B represents perpendicular planes through the same pair of lesions in the RA. Figure 4C and 4D represents magnified images shown in panels A and B, with the gap between the lesions marked using the measurement tool in Osirix.
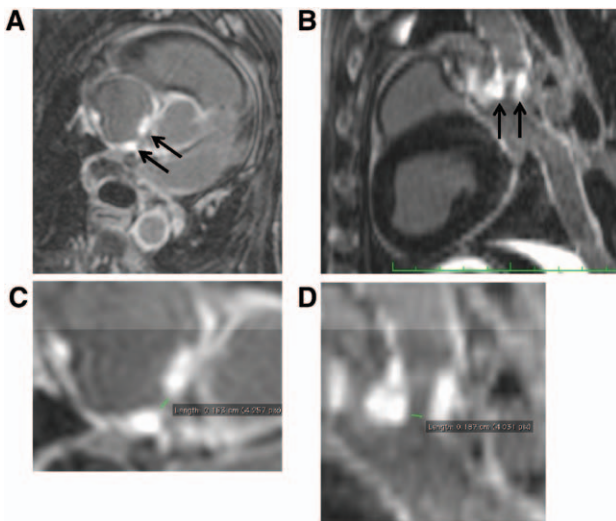

Figure 4. Late gadolinium enhancement cardiac magnetic resonance images showing ablation lesions with gap between them. **A** and **B**, Perpendicular planes showing the same ablation lesions in the right atrial wall. The ablation lesions are marked by **black arrows**. **C** and **D**, Magnified areas with the ablation lesions shown in **A** and **B**, respectively. The gap length between the lesions measured using the measurement tool in Osirix was 1.8 mm and is shown in **C** and **D**.

The gap length as determined by the gross pathology (online-only Data Supplement Figure III) was correlated with the gap length determined in the LGE MR images. Figure 5 shows the correlation between the gap length as determined by MRI, with the gap length determined by gross pathology. The correlation coefficient (R^2) is 0.95.

Discussion

Currently, when ablating for atrial fibrillation, the goal is to achieve electric isolation of all the pulmonary veins.[4] Hence, when ablating and after making the initial set of ablation lesions, the electric isolation of the pulmonary vein is checked using a functional assay typically using a multipole lasso catheter. If the veins are not electrically isolated, the lasso catheter is used to guide further ablation to isolate the veins. Using the lasso catheter allows to assess gaps that are electrically active and conducting, but it provides no feedback on the changes from ablation in the myocardial tissue itself. Furthermore, with the use of lasso catheter, one cannot identify gaps if they are electrically silent, and electric isolation has been achieved despite the presence of gaps. Other techniques such as pacing from the ablation line to capture the surrounding tissue have been reported to assess for completeness of ablation.[15] Despite the use of these tests to eliminate gaps in ablation lesion sets, pulmonary vein reconnection continues to occur over time.

In numerous studies when patients were brought back for redo procedures because of arrhythmia recurrence, the pulmonary veins isolated at the index procedures were no more electrically isolated.[7,16] The time course of recovery of conduction across previously isolated pulmonary veins is quite variable. In a human study, within just an hour after completing the pulmonary vein isolation, it was found that 30% of the pulmonary veins were reconnected.[17] Reisolating these veins resulted in an improvement in the outcome, with a lower recurrence rate for atrial fibrillation.[17] In an animal study, looking at changes in the action potential duration as a result of ablation, it was found that acutely there was a gradation in action potential changes, with the largest change occurring at the boundary of the ablated region. The action
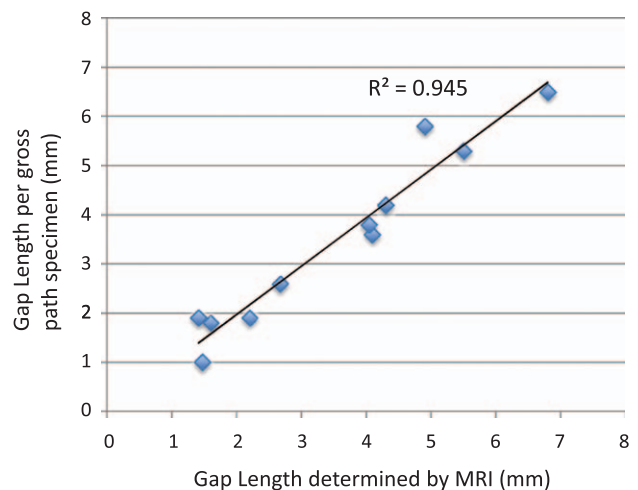

Figure 5. Correlation between gap length determined by gross pathology vs magnetic resonance imaging (MRI).

potential duration gradually approached normal ≈3 mm away from the ablation margin.[18] After about just a week, the action potential had recovered completely all the way to the edge of the ablated area.[18]

It has also been shown in an animal study that one can have electric isolation, despite the presence of gaps in myocardial tissue.[19] Using the current assay of a lasso catheter to identify and acutely target any gap areas, we miss these electrically silent gaps. Furthermore, it has been shown in a computational model that gaps, which might not be conducting acutely, can start conducting, with the recovery of some conductivity potentially leading to arrhythmia recurrence.[19] As a result, using only electric conductivity as an end point for isolation is not enough to have long-term electric isolation. To make the electric isolation more permanent, there is a need for direct visualization of changes at the tissue level from ablation and identification of gaps in the ablation lesion sets. MRI has excellent soft tissue visualization characteristics and has been used to identify ablated areas,[20] and effort has been made to develop MRI-based electrophysiology ablation system.[12,21] Here, for the first time we have used MRI to accurately identify gaps in ablation lesions immediately after ablation and then target them acutely using real-time catheter visualization. Although few other groups have attempted developing a real-time MRI system, applying it to acutely identify and target gaps in ablation lesions is novel and to the best of our knowledge has not been reported before.[22,23] This acute targeting of gaps in lesion sets will lead to more robust electric isolation by creating lesion sets without any gaps.

In conclusion, we have used the excellent soft tissue visualization capabilities of MRI to accurately identify gaps in ablation lesion sets and, then, using a real-time MRI system have shown that these gaps can be targeted acutely. This can lead to more robust ablation lesions, potentially improving clinical outcomes over time.

Limitations
The resolution of the gaps that can be detected by MRI in this study was in the millimeter range. Although submillimeter gaps are within the limits of gaps that can be tolerated in certain situations as predicted by computational models, a higher resolution will likely lead to better results.[19] This can be achieved with higher-resolution scans requiring further improvement in technology and longer scan times.

Acknowledgments

Sources of Funding

Disclosures

References
1. Aliot EM, Stevenson WG, Almendral-Garrote JM, Bogun F, Calkins CH, Delacretaz E, Della Bella P, Hindricks G, Jaïs P, Josephson ME, Kautzner J, Kay GN, Kuck KH, Lerman BB, Marchlinski F, Reddy V, Schalij MJ, Schilling R, Soejima K, Wilber D; European Heart Rhythm Association (EHRA); Registered Branch of the European Society of Cardiology (ESC); Heart Rhythm Society (HRS); American College of Cardiology (ACC); American Heart Association (AHA). EHRA/HRS Expert Consensus on Catheter Ablation of Ventricular Arrhythmias: developed in a partnership with the European Heart Rhythm Association (EHRA), a Registered Branch of the European Society of Cardiology (ESC), and the Heart Rhythm Society (HRS); in collaboration with the American College of Cardiology (ACC) and the American Heart Association (AHA). *Heart Rhythm*. 2009;6:886–933.
2. Calkins H, Brugada J, Packer DL, Cappato R, Chen SA, Crijns HJ, Damiano RJ Jr, Davies DW, Haines DE, Haissaguerre M, Iesaka Y, Jackman W, Jais P, Kottkamp H, Kuck KH, Lindsay BD, Marchlinski FE, McCarthy PM, Mont JL, Morady F, Nademanee K, Natale A, Pappone C, Prystowsky E, Raviele A, Ruskin JN, Shemin RJ; European Heart Rhythm Association (EHRA); European Cardiac Arrhythmia Scoiety (ECAS); American College of Cardiology (ACC); American Heart Association (AHA); Society of Thoracic Surgeons (STS). HRS/EHRA/ECAS expert Consensus Statement on catheter and surgical ablation of atrial fibrillation: recommendations for personnel, policy, procedures and follow-up. A report of the Heart Rhythm Society (HRS) Task Force on catheter and surgical ablation of atrial fibrillation. *Heart Rhythm*. 2007;4:816–861.
3. Cheema A, Dong J, Dalal D, Marine JE, Henrikson CA, Spragg D, Cheng A, Nazarian S, Bilchick K, Sinha S, Scherr D, Almasry I, Halperin H, Berger R, Calkins H. Incidence and time course of early recovery of pulmonary vein conduction after catheter ablation of atrial fibrillation. *J Cardiovasc Electrophysiol*. 2007;18:387–391.
4. Calkins H, Kuck KH, Cappato R, Brugada J, Camm AJ, Chen SA, Crijns HJ, Damiano RJ Jr, Davies DW, DiMarco J, Edgerton J, Ellenbogen K, Ezekowitz MD, Haines DE, Haissaguerre M, Hindricks G, Iesaka Y, Jackman W, Jalife J, Jais P, Kalman J, Keane D, Kim YH, Kirchhof P, Klein G, Kottkamp H, Kumagai K, Lindsay BD, Mansour M, Marchlinski FE, McCarthy PM, Mont JL, Morady F, Nademanee K, Nakagawa H, Natale A, Nattel S, Packer DL, Pappone C, Prystowsky E, Raviele A, Reddy V, Ruskin JN, Shemin RJ, Tsao HM, Wilber D; Heart Rhythm Society Task Force on Catheter and Surgical Ablation of Atrial Fibrillation. 2012 HRS/EHRA/ECAS expert consensus statement on catheter and surgical ablation of atrial fibrillation: recommendations for patient selection, procedural techniques, patient management and follow-up, definitions, endpoints, and research trial design: a report of the Heart Rhythm Society (HRS) Task Force on Catheter and Surgical Ablation of Atrial Fibrillation. Developed in partnership with the European Heart Rhythm Association (EHRA), a registered branch of the European Society of Cardiology (ESC) and the European Cardiac Arrhythmia Society (ECAS); and in collaboration with the American College of Cardiology (ACC), American Heart Association (AHA), the Asia Pacific Heart Rhythm Society (APHRS), and the Society of Thoracic Surgeons (STS). Endorsed by the governing bodies of the American College of Cardiology Foundation, the American Heart Association, the European Cardiac Arrhythmia Society, the European Heart Rhythm Association, the Society of Thoracic Surgeons, the Asia Pacific Heart Rhythm Society, and the Heart Rhythm Society. *Heart Rhythm*. 2012;9:632–696.e21.
5. Wilber DJ, Pappone C, Neuzil P, De Paola A, Marchlinski F, Natale A, Macle L, Daoud EG, Calkins H, Hall B, Reddy V, Augello G, Reynolds MR, Vinekar C, Liu CY, Berry SM, Berry DA; ThermoCool AF Trial Investigators. Comparison of antiarrhythmic drug therapy and radiofrequency catheter ablation in patients with paroxysmal atrial fibrillation: a randomized controlled trial. *JAMA*. 2010;303:333–340.
6. Weerasooriya R, Khairy P, Litalien J, Macle L, Hocini M, Sacher F, Lellouche N, Knecht S, Wright M, Nault I, Miyazaki S, Scavee C, Clementy J, Haissaguerre M, Jais P. Catheter ablation for atrial fibrillation: are results maintained at 5 years of follow-up? *J Am Coll Cardiol*. 2011;57:160–166.
7. Ouyang F, Antz M, Ernst S, Hachiya H, Mavrakis H, Deger FT, Schaumann A, Chun J, Falk P, Hennig D, Liu X, Bänsch D, Kuck KH. Recovered pulmonary vein conduction as a dominant factor for recurrent atrial

tachyarrhythmias after complete circular isolation of the pulmonary veins: lessons from double Lasso technique. *Circulation*. 2005;111:127–135.

8. Cappato R, Negroni S, Pecora D, Bentivegna S, Lupo PP, Carolei A, Esposito C, Furlanello F, De Ambroggi L. Prospective assessment of late conduction recurrence across radiofrequency lesions producing electrical disconnection at the pulmonary vein ostium in patients with atrial fibrillation. *Circulation*. 2003;108:1599–1604.

9. Melby SJ, Lee AM, Zierer A, Kaiser SP, Livhits MJ, Boineau JP, Schuessler RB, Damiano RJ Jr. Atrial fibrillation propagates through gaps in ablation lines: implications for ablative treatment of atrial fibrillation. *Heart Rhythm*. 2008;5:1296–1301.

10. Dickfeld T, Kato R, Zviman M, Lai S, Meininger G, Lardo AC, Roguin A, Blumke D, Berger R, Calkins H, Halperin H. Characterization of radiofrequency ablation lesions with gadolinium-enhanced cardiovascular magnetic resonance imaging. *J Am Coll Cardiol*. 2006;47:370–378.

11. Dickfeld T, Kato R, Zviman M, Nazarian S, Dong J, Ashikaga H, Lardo AC, Berger RD, Calkins H, Halperin H. Characterization of acute and subacute radiofrequency ablation lesions with nonenhanced magnetic resonance imaging. *Heart Rhythm*. 2007;4:208–214.

12. Vergara GR, Vijayakumar S, Kholmovski EG, Blauer JJ, Guttman MA, Gloschat C, Payne G, Vij K, Akoum NW, Daccarett M, McGann CJ, Macleod RS, Marrouche NF. Real-time magnetic resonance imaging-guided radiofrequency atrial ablation and visualization of lesion formation at 3 Tesla. *Heart Rhythm*. 2011;8:295–303.

13. Kim RJ, Fieno DS, Parrish TB, Harris K, Chen EL, Simonetti O, Bundy J, Finn JP, Klocke FJ, Judd RM. Relationship of MRI delayed contrast enhancement to irreversible injury, infarct age, and contractile function. *Circulation*. 1999;100:1992–2002.

14. Weiss C, Stewart M, Franzen O, Rostock T, Becker J, Skarda JR, Meinertz T, Willems S. Transmembraneous irrigation of multipolar radiofrequency ablation catheters: induction of linear lesions encircling the pulmonary vein ostium without the risk of coagulum formation? *J Interv Card Electrophysiol*. 2004;10:199–209.

15. Eitel C, Hindricks G, Sommer P, Gaspar T, Kircher S, Wetzel U, Dagres N, Esato M, Bollmann A, Husser D, Hilbert S, Zaker-Shahrak R, Arya A, Piorkowski C. Circumferential pulmonary vein isolation and linear left atrial ablation as a single-catheter technique to achieve bidirectional conduction block: the pace-and-ablate approach. *Heart Rhythm*. 2010;7:157–164.

16. Segerson NM, Daccarett M, Badger TJ, Shabaan A, Akoum N, Fish EN, Rao S, Burgon NS, Adjei-Poku Y, Kholmovski E, Vijayakumar S, DiBella EV, MacLeod RS, Marrouche NF. Magnetic resonance imaging-confirmed ablative debulking of the left atrial posterior wall and septum for treatment of persistent atrial fibrillation: rationale and initial experience. *J Cardiovasc Electrophysiol*. 2010;21:126–132.

17. Wang XH, Liu X, Sun YM, Gu JN, Shi HF, Zhou L, Hu W. Early identification and treatment of PV re-connections: role of observation time and impact on clinical results of atrial fibrillation ablation. *Europace*. 2007;9:481–486.

18. Wood MA, Fuller IA. Acute and chronic electrophysiologic changes surrounding radiofrequency lesions. *J Cardiovasc Electrophysiol*. 2002;13:56–61.

19. Ranjan R, Kato R, Zviman MM, Dickfeld TM, Roguin A, Berger RD, Tomaselli GF, Halperin HR. Gaps in the ablation line as a potential cause of recovery from electrical isolation and their visualization using MRI. *Circ Arrhythm Electrophysiol*. 2011;4:279–286.

20. Badger TJ, Daccarett M, Akoum NW, Adjei-Poku YA, Burgon NS, Haslam TS, Kalvaitis S, Kuppahally S, Vergara G, McMullen L, Anderson PA, Kholmovski E, MacLeod RS, Marrouche NF. Evaluation of left atrial lesions after initial and repeat atrial fibrillation ablation: lessons learned from delayed-enhancement MRI in repeat ablation procedures. *Circ Arrhythm Electrophysiol*. 2010;3:249–259.

21. Schmidt EJ, Mallozzi RP, Thiagalingam A, Holmvang G, d'Avila A, Guhde R, Darrow R, Slavin GS, Fung MM, Dando J, Foley L, Dumoulin CL, Reddy VY. Electroanatomic mapping and radiofrequency ablation of porcine left atria and atrioventricular nodes using magnetic resonance catheter tracking. *Circ Arrhythm Electrophysiol*. 2009;2:695–704.

22. Lardo AC, McVeigh ER, Jumrussirikul P, Berger RD, Calkins H, Lima J, Halperin HR. Visualization and temporal/spatial characterization of cardiac radiofrequency ablation lesions using magnetic resonance imaging. *Circulation*. 2000;102:698–705.

23. Nordbeck P, Bauer WR, Fidler F, Warmuth M, Hiller KH, Nahrendorf M, Maxfield M, Wurtz S, Geistert W, Broscheit J, Jakob PM, Ritter O. Feasibility of real-time MRI with a novel carbon catheter for interventional electrophysiology. *Circ Arrhythm Electrophysiol*. 2009;2:258–267.

CLINICAL PERSPECTIVE

The goal in most ablation procedures is to electrically isolate one region from another by creating a set of contiguous and transmural ablation lesions. Yet, despite the best effort of electrophysiologists, gaps remain in ablation lesion sets. This stems from the fact that when ablating there is no direct visualization of ablation-related tissue changes and ablation is inferred based on numerous indirect parameters. Magnetic resonance imaging (MRI) has excellent soft tissue visualization characteristics, and in this study, this property of MRI was used to acutely identify ablation lesions and in turn identify the gaps between ablation lesions. A challenge in using MRI for ablation is that the currently used ablation catheters are not MRI compatible. For this study, MRI-compatible electrophysiology mapping and ablation catheters were developed. A complete real-time MRI-based electrophysiology system was also developed by integrating the use of MRI-compatible catheters with real-time imaging. This system was used to acutely identify the ablation lesions, the gaps in between the lesions, and then target the gaps acutely. An MRI-based electrophysiology system not only does away with exposure of ionizing radiation to the patient and the operator but also allows direct visualization of tissue changes, with ablation potentially leading to significant improvement in ablation procedure outcomes.

SUPPLEMENTAL MATERIAL
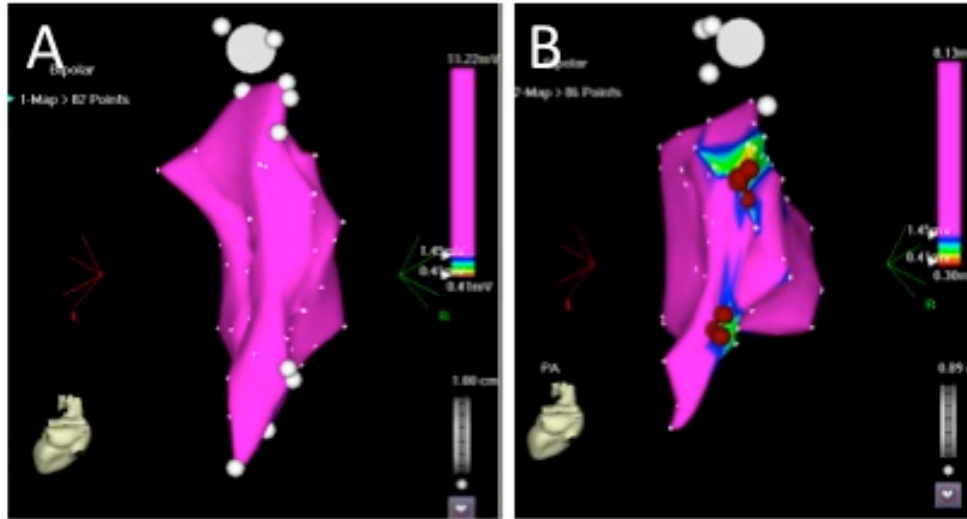
CARTO voltage map made before and after creating lesions in the posterior wall of the right atrium. Panel A is a baseline bipolar voltage map of the right atrium showing no areas of low voltage. A PA view of the right atrium is shown. Panel B is a voltage map made after two discrete ablation lesions. The ablated area is marked by red dots. The voltage map confirms areas of low voltage around the ablation lesions. The bi-polar voltage color scale is shown on the top right hand corner of panels A and B.
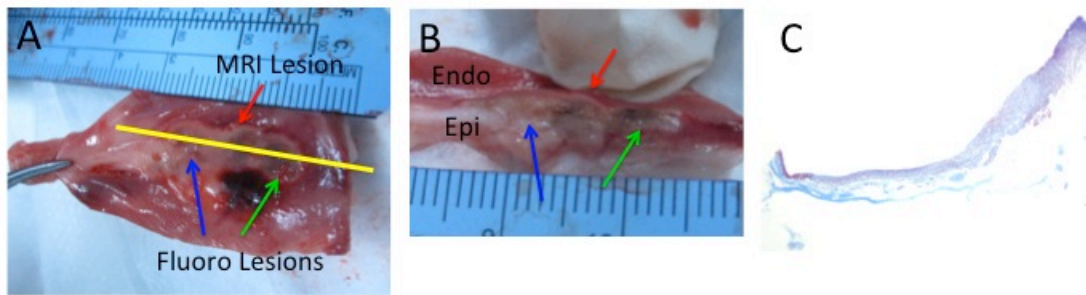
Gross pathology and histology of right atrial tissue showing ablation lesions after
the gap area was ablated in the MR scanner. Panel A is gross tissue specimen
showing the two lesions made in the EP lab using fluoroscopy (blue and green
arrows) and the gap area ablated in the MR scanner (red arrow). The yellow line in
panel A is the plane of cut section shown in panel B. Panel B is a cut section through
the ablation lesions showing the transmurality of the lesions. Endo and epi mark the
endocardial and the epicardial surfaces of the tissue specimen. Panel C is a Masson's
Tichrome stained tissue specimen from panel B showing the lack of any red stained
areas in the middle of the section confirming the transmurality of the ablation
lesions.
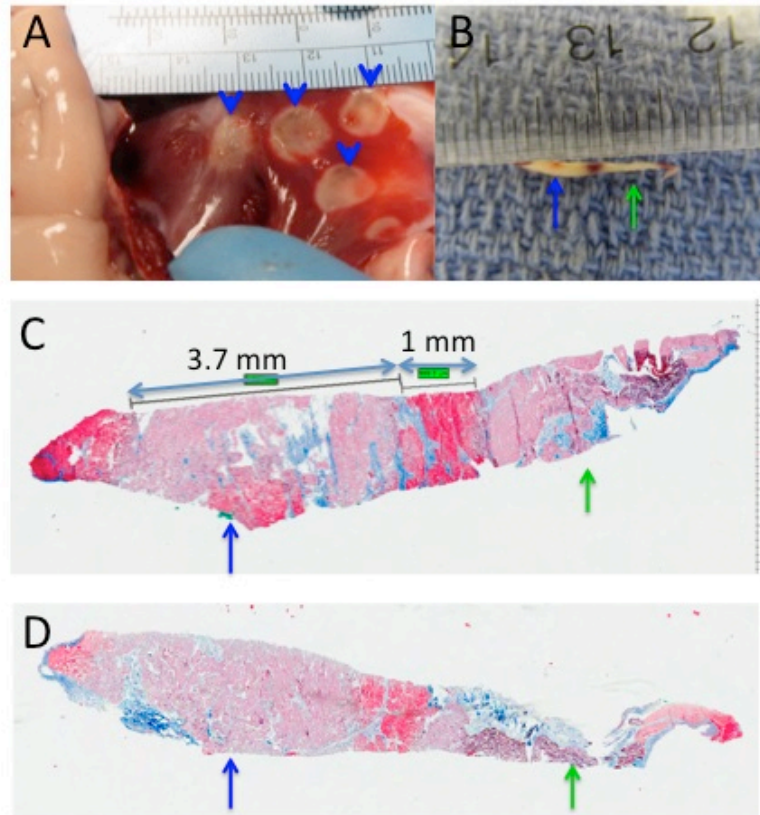
Gross pathology and histology of atrial tissue showing ablation lesions with gaps of varying lengths. Panel A shows ablation lesions (marked by arrowheads) made in the right atrium spaced 1 to 4 mm apart. Panel B is a gross tissue section with two ablation lesions and a gap of 1 mm from another animal. Panel C is tissue shown in panel B stained with Masson's Trichrome confirming the ablation lesion and the 1 mm gap in between. Panel D is another section from the same block as in C confirming the transmurality of the left sided lesion.